4th International Workshop on Microsystems

Alexander Campus, International Hellenic University, 18 December 2019

Workshop Proceedings

Introduction

This workshop brings together research and development from a large spectrum of science and engineering fields related to the implementation of microsystems in the new era of distributed information technologies. As cloud computing services and smart portable systems are becoming ubiquitous and more advanced, new possibilities for interdisciplinary research emerge. The microsystems that comprise the so-called internet of things will encompass a wide range of technologies including new energy sources, energy and information electronics, sensor systems, smart and energy efficient control and computing, telecommunications and networking, and also nanotechnology and micro-electro-mechanical systems. Continuing three successful workshops in 2016, 2017 and 2018, the 4th International Workshop on Microsystems aims at bringing together related research and development advancements from the academic community and the industry. Scientific topics include but are not limited to:

Energy microsystems	Industrial automation and control
Sensors and sensor electronics	Microelectronics and nanoelectronics
Embedded systems	Micro-electro-mechanical systems
Integrated Circuits and Systems	Computing for microsystems

Michail E. Kiziroglou
m.kiziroglou@autom.teithe.gr

Venue

Lecture Theater, Automation and Informatics Building
Sindos Campus, ATEI Thessaloniki, Greece

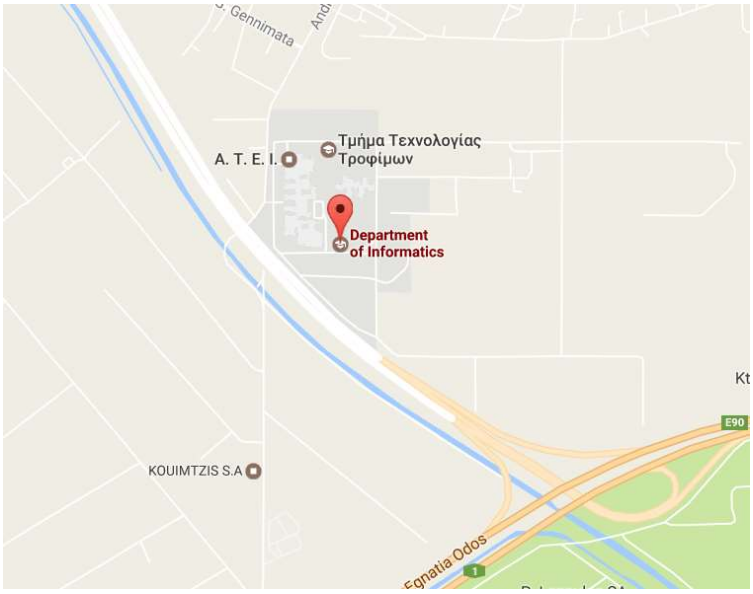

Date

Wednesday, 18th of December, 2019

Organizer

Michail E. Kiziroglou

Session Chairs

Dr. Kostas Siozios, Dep. of Physics, AUTH
Dr. Georgios Andreou, Dep. Electrical and Computer Eng., AUTH

Reviewing Committee

Dimitrios Bechtsis
Maria Drakaki
Chrisovalantou Ziogou
Michail E. Kiziroglou
Simira Papadopoulou
Fotis Stergiopoulos
Dimitris Triantafyllidis
Kostas Siozios
Apostolos Tsagaris
Christos Yfoulis

Organization and Technical Support

Kostantinos Pakas and Maria Pagkrakioti

List of Authors

No	Last Name	First Name / Initials	Affiliation
1	Athanasiadis	F.	IHU
2	Bechtsis	Dimitrios	IHU
3	Boyle	David E.	Imperial College London
4	Charitonidis	A.	IHU
5	Evgenidis	N	IHU
6	Filelis	A.	Evresis S. A.
7	Geladaris	Theodoros	Semitron S.A.
8	Kiziroglou	Michail E.	IHU, Imperial College London
9	Kosmanis	Theodoros	IHU
10	Kritikou	E.	IHU
11	Loukovitis	Ioannis	AUTH
12	Manolas	A.	IHU
13	Nikolaidis	Nikolaos	IHU
14	Pandiyan	Akshayaa	Imperial College London
15	Papaoikonomou	S.	Evresis S. A.
16	Papavassiliou	Christos	Imperial College London
17	Stergiopoulos	Fotis	IHU
18	Triantafyllidis	Dimitris	IHU
19	Tsagaris	Apostolos	IHU
20	Tsalikis	Dimokratis	IHU
21	Tsirtou	P.	IHU
22	Vamvatiras	Dimitris	Semitron S.A.
23	Wright	Steven W.	Imperial College London
24	Yeatman	Eric M.	Imperial College London
25	Yfoulis	Christos	IHU

Programme

08:45-09:15: Registration

Please check-in or register at the front desk

09:15-09:30: Welcome and introduction

09:30-10:45: First Oral Session (Session Chair: Dr. Konstantinos Siozios, AUTH)

09:30 – 10:15: Engineering the Nanoscale: Turning defects into features. *Dr. Christos Papavassiliou, Imperial College London,* 19WOM-01 (keynote).

10:15: Practical PID servo control of a laboratory single-jointed propeller arm using low-cost embedded control hardware and software. *I. Loukovitis and Ch. Yfoulis*, 19WOM-02

10:30: Development and modeling of a battery system for commercial electric bicycles, *A. Charitonidis, F. Athanasiadis, A. Manolas, P. Tsirtou, E. Kritikou, T. Kosmanis*, 19WOM-03

10:45-11:15: Coffee Break and Poster Session

Configurable voltage transformation for energy harvesting with the LTC3109 IC, *D. Tsalikis and M. E. Kiziroglou*, 19WOM-04.

11:15-12:30: Second Oral Session (Session Chair: Dr. Georgios Andreou, AUTH)

11:15: Embedded Systems from Industry's view, *D. Vamvatiras and Th. Geladaris*, 19WOM-05

12:00: Prototype Power Supply Solutions for a Gel Electrophoresis Apparatus, *D. Triantafyllidis, N. Nikolaidis, N. Evgenidis, D. Bechtsis, Ap. Tsagaris, A. Filelis, S. Papaoikonomou and F. Stergiopoulos,* 19WOM-06

12:15: Acoustic Power Transfer Through Structures, M. E. Kiziroglou, A. Pandiyan, D. E. Boyle, S. W. Wright and E. M. Yeatman, 19WOM-07

12:30-13:00: Best Paper Award by Ioannidis Electronics. Concluding remarks.

WORKSHOP ABSTRACTS

Engineering the Nanoscale: Turning defects into features (Invited)

Christos Papavassiliou

Dept of Electrical and Electronic Engineering, Imperial College London

A dreaded enemy of CMOS technology is gate leakage, initiated by a dielectric breakdown of the gate insulator. Breakdown becomes increasingly likely as dimensions shrink, gate oxides are reduced to a thickness of a few atoms and exotic materials are used to raise the gate insulator dielectric constant in order to maximise transistor gain. Dielectric breakdown is indeed the nightmare of young PhD students struggling to learn how to make microelectronics devices, and of IC design engineers whose CMOS integrated circuits frequently die of electrostatic breakdown during manufacture.

The novel, very promising, devices called memristors, are nanoscale devices whose resistance changes to record the history of signals applied on them. Memristors are thin oxide layers destroyed by dielectric breakdown. The leaky gate oxides of yesteryear are starting to be useful for information storage, both digital and analog!

In this talk we will talk about Memristors; we will show one way to turn dielectrically destroyed capacitors to useful devices. A design methodology for configurable circuit elements for use in Field Programmable Analogue Arrays is introduced. Memristors are used as analogue memories for the configuration information of adjustable monolithic circuit components, e.g. inductors, capacitors and gain elements. Memristor-enabled tuneable blocks have the potential to simplify the design of Field Programmable Analogue Arrays, increase their functionality and, as a result, promote their use. The discrete implementations of reconfigurable components achieve over a decade of component value adjustment range, and operational frequencies to 10s or even 100s of MHz. Both component adjustment range and other performance metrics are expected to significantly increase in eventual monolithic implementations.

Practical PID servo control of a laboratory single-jointed propeller arm using low-cost embedded control hardware and software

Ioannis Loukovitis and Christos Yfoulis

***Abstract*— This paper presents an experimental setup developed in the thesis work of the first author. The project focused on the modeling and the position control of a custom-built propeller-arm system which can swing between 0º and 180º around an axis fastened on a wooden, L-shaped base. Due to the fact that the system behaves similarly to a pendulum, the non-linearity of the system is strongly visible even in changes between a small range of angles which makes this particular system a good candidate for an undergraduate control laboratory experiment. It provides useful modeling and control design experimentation opportunities with practical PID control laws, which are often disregarded in the educational curriculum of a typical undergraduate control laboratory. The total cost of construction and development has been kept extremely low due to the adoption of modern, popular low-cost hardware and software Arduino-based platforms, compatible sensors and recycled materials.**

Key words – Control education; Control courses and labs; Arduino lab; practical PID; servo control;

I. INTRODUCTION

Recent years have witnessed the popularity of a new trend for control system laboratories, i.e. the development of low-cost take-home equipment [1]. The main reason is that significant flexibility is offered and the student's needs are better integrated. This trend has evolved alongside the recent advances in microcontroller and internet technology which led to the availability of low-cost microprocessors such as Arduino or Raspberry Pi, hugely supported by a growing community of users, hobbyist and developers. The result is a significant reduction of time and cost for the development of software and hardware platforms for embedded control. Control education can certainly benefit from these recent advances [2], not only in small but also in medium-scale applications and equipment. Especially the teaching of the *Proportional-Integral-Derivative (PID)* control laws family, which constitute the most useful and popular industrial standard, suffers from this policy and is not getting the attention it deserves [4]. The equipment described in this paper is a custom-built propeller-arm system, shown in Fig. 1, which has been constructed at a very reasonable cost of approximately 30 Euros in the thesis work of the first author [3], and under the supervision of the second author. It offers increased and more interesting possibilities for teaching the basics of *practical PID control,* in the presence of *nonlinearities and sensor noise*, while offering *disturbance rejection* properties. It allows straightforward exposition and direct experimentation with extra features such as derivative term filter, anti-windup control, set-point weighting, Kalman filter, etc. Furthermore, first principles as well as black-box modeling and identification is possible, supporting the teaching needs of other undergraduate courses.

* Ioannis Loukovitis is a Theoretical Informatics and Systems & Control Theory postgraduate student of the Department of Mathematics, AUTH/GREECE (email: ioloukov@math.auth.gr). Christos A. Yfoulis is an associate professor with IEM/IHU, GREECE (phone: 2310013994; fax: 2310791131; e-mail: cyfoulis@autom.teithe.gr).

II. A CUSTOM-BUILT SINGLE-JOINTED PROPELLER ARM

The project began with the construction of an L-shaped wooden base to which a metallic hinge/arm is attached. Moreover, at the end of the arm, a Micro-Electro-Mechanical-System (*MEMS*) sensor module is mounted. The motor is supplied by a DC source through a circuit called Electronic Speed Controller (*ESC*), responsible for generating a suitable three-phase signal and the sensorless control of the brushless DC (BLDC) motor's speed. The Micro-Controller Unit (*MCU*) is an *Arduino UNO* and the power supply is a recycled PC PSU unit (see Fig. 1).

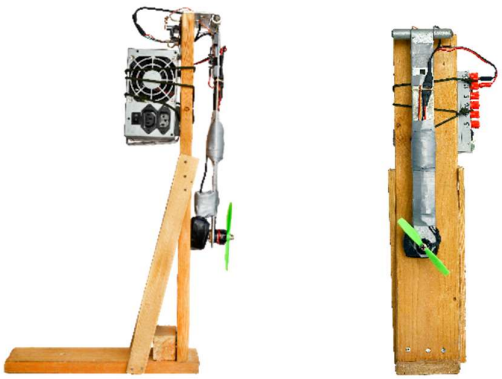

Fig. 1 The custom-built construction, side and front view

Physical system modeling

We start by modeling the free body as a pendulum [5] in which the acting forces are its own weight and the reaction at the rotational joint, which is modeled with the following unforced equation of motion

$$-(M+m)gl_G \sin\theta - b\dot{\theta} = I_O\ddot{\theta} \qquad (1)$$

Experimental identification

The next step is to acquire data from an open-loop response bringing the arm at rest around 45º as seen in Fig. 2 and employ the *logarithmic decrement* to derive the damping ratio $\zeta = 0.065$ and the natural frequency $\omega_n = \frac{\omega_d}{\sqrt{1-\zeta^2}} = 5.6756\frac{rad}{sec} \cong \omega_d$ since ζ is very small. We continue with the estimation of the pendulum's mass moment of inertia and the viscous friction constant b and finally, by taking into account the dc-gain of the data used in Fig. 2 we arrive at an approximate transfer function (TF)

$$G(s) = \frac{0.625}{0.0357s^2+0.0264\,s+0.81359} \left(= \frac{M}{s^2+p\,s+q}\right) \qquad (2)$$

A comparison between the experimental and simulated data in MATLAB/SIMULINK is depicted below in Fig. 2.

III. PID DESIGN AND PRACTICAL IMPLEMENTATION

We adopt a systematic, analytical approach for a successful control design that can deal with set-point tracking and

disturbance rejection at the same time with maximum efficiency. For an open-loop system with TF (2) and a PID controller in the following typical "academic" form

$$C(s) = K_p + \frac{K_i}{s} + K_d s = \frac{K_d s^2 + K_p s + K_i}{s} \quad (3)$$

we place the three closed-loop poles according to the optimal Integral-Time-Absolute-Error (ITAE) criterion [6], i.e. adopting a desired prototype third order polynomial

$$P_3(s) = s^3 + 1.75\,\omega_n\,s^2 + 2.15\,\omega_n^2\,s + \omega_n^3 \quad (4)$$

and equating the corresponding coefficients of the closed loop TF, which provides the following solution

$$K_d = \frac{1.75\,\omega_n - p}{M},\ K_p = \frac{2.15\,\omega_n^2 - q}{M},\ K_i = \frac{\omega_n^3}{M} \quad (5)$$

where ω_n is a free design parameter that can be increased within the system's physical limitations while it is proportional to the system's bandwidth.

The ITAE PID controller has produced a controllable system up to the point of the system's limitations due to non-linearity (around 100° maximum), that is very well capable of quickly rejecting large disturbances with very satisfactory rise and settling times as shown in the following Figs. 3-5. It is also clear that the magnitude of the step change does not affect the system performance at all, as we see minimal-to-none overshoot, even for a 90° change.

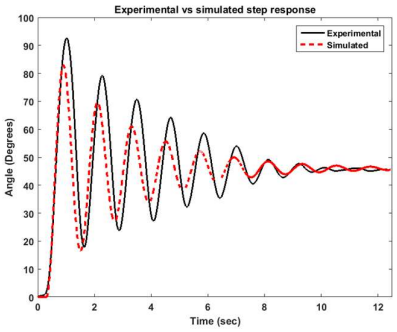

Fig. 2 Experimental vs simulated step response

It is noteworthy to mention that these nice results are not obtained with a simple "*theoretical*" control law implementation as in (5). A number of additional features and implementation details, which remain invisible to students, play a crucial role. A "*practical*" PID controller is implemented in the following general form

$$u(t) = K_p\big(b\,r(t) - y(t)\big) + K_i \int e(\tau)\,d\tau + K_d\left(-\frac{dy_f(t)}{dt}\right) \quad (6)$$

with a set-point weighting parameter b and a filtered derivative action with a filter parameter N given by

$$\frac{T_d}{N}\frac{dy_f(t)}{dt} + y_f(t) = y(t)\ ,\ T_d = K_p/K_d \quad (7)$$

The set-point (reference) weighting parameter b can be used to obtain a pseudo 2 degree of freedom (DOF) structure, i.e. a simple means to separate disturbance rejection from response to reference signals [4]. Alternatively, a 2DOF structure with a *prefilter* can be designed [6]. A typical integrator *anti-windup* mechanism is also included. It is worth noting that (6) employs the so-called "*derivative in measurement*" idea, which places the derivative action to the feedback path, hence avoiding spiking during abrupt reference changes. The best results in our system have been obtained by the so-called *I-PD* controller form, where the P,D parts are implemented in feedback, i.e. as in (6) with $b = 0$. The derivative filter is widely used in practice to suppress the effect of noise and the spiking that can be induced from differentiating noisy sensor data, as well the introduction of vibrations in mechanical systems. The usage of a Kalman filter with our gyro sensor was found absolutely necessary for proper control in the noisy environment created by the motor and propeller. The experimental results presented in Figs. 3-5 have been obtained using the standard *Arduino PID* and *Kalman filter* libraries publicly available.

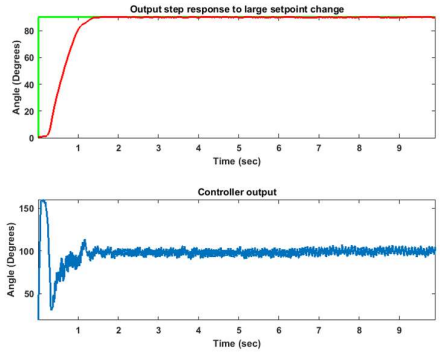

Fig. 3 ITAE PID controller, step response 0-90°, ω_n=8 rad/sec

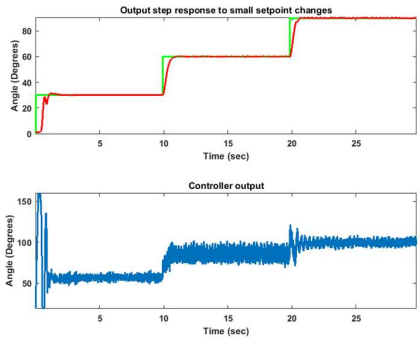

Fig. 4 ITAE PID controller, step response, ω_n=8 rad/sec

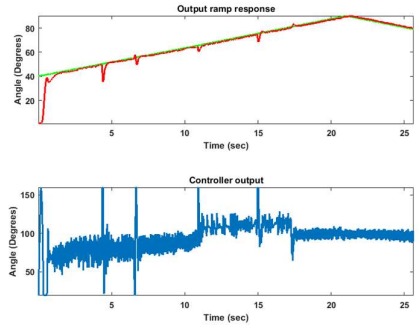

Fig. 5 ITAE PID controller, ramp response, ω_n=8 rad/sec

References

[1] B. Taylor, P. Eastwood & B. Ll. Jones, "Development of a Low- cost, Portable Hardware Platform to Support Hands-on Learning in the Teaching of Control and Systems Theory", *Engineering Education* Vol. 9, Iss. 1, 2014.

[2] Jaroslav Sobota, Roman PiSl, Pavel Balda, MiloS Schlegel, "Raspberry Pi and Arduino boards in control education", *IFAC Proceedings Volumes,* Volume 46, Issue 17, 2013, pp. 7-12.

[3] I. Loukovitis, Bachelor Thesis, «Construction and control of a single-jointed propeller arm», Dpt of Automation Engineering, ATEI of Thessaloniki, October 2018.

[4] K.J. Astrom, Tore Hagglund. Advanced PID Control, ISA-The Instrumentation, Systems, and Automation Society, 2006.

[5] Mathworks, "Control tutorials for MATLAB and SIMULINK, hardware activities, Activity 3: modeling of a simple pendulum", http://ctms .engin. umich. edu/CTMS/index. php?

[6] R.C. Dorf, R.H. Bishop, Modern Control Systems, Prentice Hall, 12th ed., 2011.

Development and modeling of a battery system for commercial electric bicycles

A. Charitonidis, F. Athanasiadis, A. Manolas, P. Tsirtou, E. Kritikou and T. Kosmanis

International Hellenic University, Department of Industrial Engineering and Management, 57400, Sindos, Greece

Abstract— **The development of a battery system appropriate for electric bicycles is the subject of this paper. Oriented to be implemented as a plug-and-play equipment in existing electric bicycles or as part of a conversion kit, the analyzed battery system can successfully support electric and electric power assisted bicycles providing simultaneously real time information about critical powertrain parameters like battery and cell voltages, currents, temperatures and battery state of charge (SoC). A series of on the road experiments are used to evaluate the performance of the battery system. Additionally, the overall powertrain of the bicycle is modeled in order to compare the real world performance with simulation results.**

Index Terms*— *Electric bicycles, energy storage system, battery modeling

I. Introduction

THE intrusion of vehicle electrification in the world of the so-called human powered vehicles like bicycles and various types of tricycles was inevitable. The initial power assistance offered to the riders has become autonomous electric traction but at the same time the safe, speed limited, due to the restricted power a human can or is willing to provide, vehicles have become more demanding in terms of power delivery, operation monitoring and driving range [1]-[2]. From the architectural point of view, the electric bicycle significantly differs from other types of electric vehicles since it is not in general a purely electric vehicle. It actually is a hybrid electric vehicle, the second source of traction power delivered to the wheels by the rider (human). Although pure electric traction is possible in electric bicycles, the most interesting case is that of the pedelec, that is the electrically power assisted bicycle. This is considered to be hybrid electric vehicle of parallel configuration where human power and electricity can at the same time contribute to bicycle traction.

Initial batteries used for transforming conventional human powered vehicles into electric ones have been found in many cases inadequate regarding power delivery, power density, operation range, life, even safety [2]. That is the reason why they are considered to be the most critical structure of the electrical powertrain. On the other hand, lack of international standards regarding electric vehicle batteries also affect the market of electric bicycles and allow a great deal of freedom to manufacturers in order to develop high performance products.

The battery system presented in the next section, has been developed in order to meet the requirements of modern human powered vehicles, and not only support electrical assistance. It is also meant to be free of the aforementioned deficiencies and to allow detailed and continuous monitoring of critical parameters like cell temperature, electric current, cell and battery voltages as well as real time estimation of the battery state of charge. High energy, high power cells are utilized in order to assure good range when traction power is purely electric and good performance in increased load situations. The developed battery system, continuously balanced and monitored, has been undergone a series of on road experiments empowering an electric bicycle in order to prove its efficiency. The resulted system has also been simulated by means of a first order equivalent circuit. The rest of the powertrain has been simulated with the aid of the traction equation. Comparison of the measurement and simulation results regarding battery voltage and state of charge present adequate convergence.

II. Energy Storage System Development

The overall battery system is composed of the battery cells stack, a passive battery management system (BMS) to ensure cell balancing during charging and discharging, a temperature measurement circuit, a controller, monitoring battery operation, and a display. As it is developed to provide electric power to human powered vehicles, it was initially selected to be adjusted to the electric bicycle of Fig. 1, supporting 5 levels of electrical assistance for the rider and meeting the requirements of current European legislation [3], that is not exceeding the speed of 25km/h. Assuming a bicycle rider of 85-115kg and taking into account the fact that, on a typical asphalt flat road, 50Wh provide a range of 10km, bicycle autonomy was selected to be around the average value of 50 km [2]. The degrees of freedom in the design focus on the battery system, which determines bicycle autonomy, assuming it is solely electrically powered, and all monitoring parameters. Thus, the battery was designed with a nominal capacity around 14Ah and nominal voltage 36V, equal to the nominal voltage of the electric motor selected.

Fig. 1. Battery system components and their spatial placing on the e-bike.

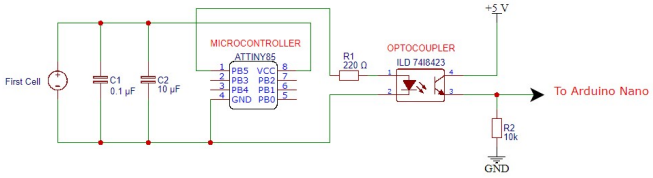

Fig. 2. Voltage measurement circuit across a typical battery cell.

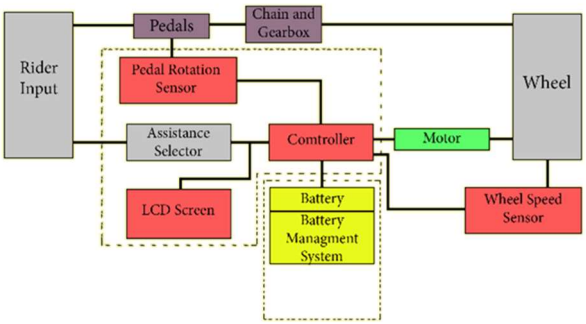

Fig. 3. Block diagram of the battery pack system.

The cell types selected for the battery pack are the Panasonic NCR18650PF Li-ion 18650 cells [4], having as nominal specifications 3.6V voltage, 2900mAh capacity, 1C discharge rate and 3.5C maximum continuous discharge rate. In order for the overall battery to provide 36V voltage and about 14Ah capacity (14.5 to be precise), fifty cells were connected in a 10s5p structure. This kind of structure is able to provide 14.5A nominal discharge current and 50.75A maximum continuous current to the motor, values that are considered adequate for the operation of the electric motor selected. The battery cell pack was cold welded by means of aluminum foils and enclosed in a 3D printed case made of biological Polylactic Acid (PLA) filament, appropriately designed so as to fulfill all technical and space limitations. Together with the battery itself, the temperature measurement circuit as well as the BMS were installed in the PLA enclosure, thus forming the complete battery pack (green structure of Fig. 1).

The measuring and monitoring system records the crucial measures connected to the battery, that is cell voltage for all battery cells, overall battery voltage, battery discharging and charging current, temperature per cell and ambient temperature are measured instantaneously, allowing complete monitoring of battery's state of operation. These values are utilized for the calculation of the instantaneous State of Charge (SoC) which appears on the indication display located on the steering wheel of the bicycle as shown in Fig. 1 and Fig. 3.

The monitoring system was based on three sensor circuits, measuring voltage, temperature and electric current. For the monitoring of the voltage of each cell as well as of the overall battery pack, the circuit of Figs. 3 and 5 was developed based on the microcontroller ATTINY 85 and optocoupler in order to isolate the processor (Arduino Nano) from the rest of the circuitry. Cell temperature was performed by means of ten digital temperature sensors Dallas DS18B20 directly connected to bicycle's main controller, an Arduino MEGA one (Fig. 3). Finally, an ACS 712 current sensor connected in series with negative pole of the battery provided the instantaneous value of electric current. Current measurement is exploited not only to assure protection of the battery pack but also in order to allow instantaneous battery SoC estimation. The latter is considered to be a crucial parameter for the rider as well as for the comparison with simulation data.

Instantaneous SoC calculation is based on a Coulomb counting procedure combined with an initial SoC estimation through a piecewise relationship with the battery Open Circuit Voltage (OCV) [5]. Particularly, each time the battery is about to deliver power to the motor after a non-operational time interval, the OCV is measured and corresponded to a SoC value, that is assumed to be the initial SoC, $SoC(t_0)$. The electric charge, $dQ(t)$, leaving the battery pack during the discharging procedure is measured by the Coulomb counting procedure as described by the following equation and approximated by the summation of elementary charges $i_k \delta t$

$$dQ(t) = \int_0^t i(t)dt = \sum_k i_k \delta t \quad (1)$$

where i_k is assumed to be constant in the time interval δt. Therefore, the repetitive measurement of electric current leaving the battery is enough to allow the update of the battery SoC value according to

$$SoC(t) = SoC(t_0) - dQ(t)/Q_{nom} \quad (2)$$

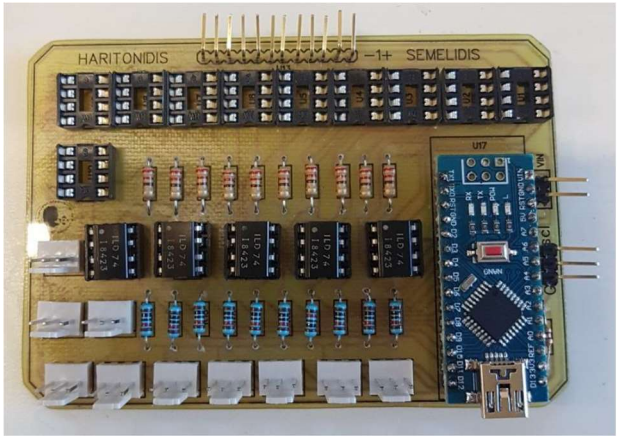

Fig. 4. Voltage and temperature measurement PCB.

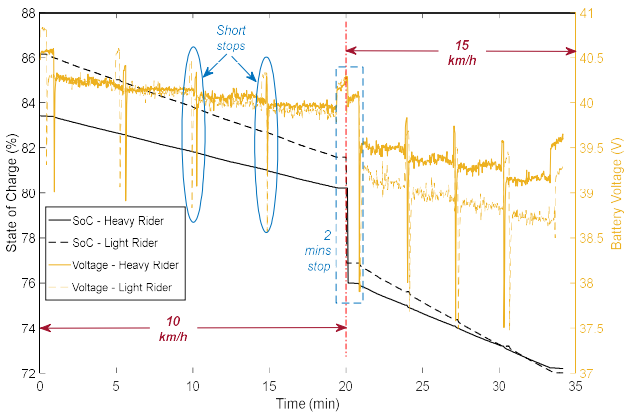

Fig. 5. Battery SoC and voltage vs speed and rider weight.

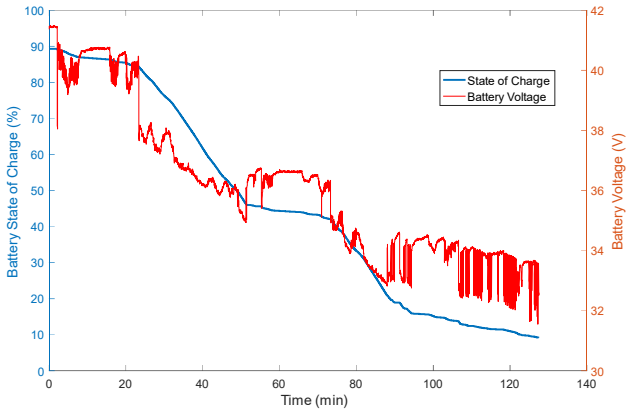

Fig. 6. Battery SoC and voltage during range testing.

where Q_{nom} is the nominal capacity of the battery pack. Apparently, during charging procedure the sign in front of the fracture becomes positive.

The instantaneous *SoC* is recorded together with all other measured values on a memory disc during measurement phases, and depicted on the bicycle information display (Fig. 3). Also, together with the instantaneous values of battery pack voltage, it is utilized for comparison with simulation data.

III. Measurement and Simulation

The performance of the battery system was evaluated through a series of measurement tests conducted on the electric bicycle with the aid of the special measuring device that was consisted of an appropriately developed PCB circuit of Fig. 4 and a data acquisition software. As described in the previous section, the overall measuring system was attached to the bicycle during the tests allowing the measurement and recording of voltages, currents and temperatures measured by the bicycle monitoring system as well as SoC calculated as previously described.

The experiments performed were divided into two types. The first type aimed in testing bicycle performance under various loads caused either by the overall weight of the bicycle and rider either by the speed profiles of the bicycle. The bicycle was ridden by four different riders, weighting about 56kg, 72kg, 85kg and 114kg with the bicycle, covering four times a rectangular, closed 750m long, pathway. The circuit, having overall length 3km, was covered at four different constant speeds. Thus, 16 different bicycle load profiles were created. Fig. 5 presents the variation of battery state of charge and voltage for the heavier and light rider and bicycle speed at 10km/h and 15km/h. Battery voltage presents very slight alterations as the battery SoC diminishes with time, as demanded. The voltages drops observed at short stops are connected to the high current the motor requires every time it restarts. Similar figures can be contacted for all load profiles.

Additionally, a range test of the bicycle was performed on a straight and flat road with an average rider at a relatively constant maximum speed (25km/h) without pedaling. Two bicycle-rider weights were selected, at 85kg and 114kg. In both cases the bicycle was ridden for 50km for a total time of about 2h. The battery energy consumed was 76.8% and 80.14% respectively without voltage reduction below critical levels (2.5V), allowing the safe assumption that the bicycle range is 50km. As depicted in Fig. 6, where the variation of battery SoC and voltage with time is shown for the case of a heavy rider over a two hour riding, voltage ranges from 41.5V maximum to 32V minimum which as the SoC ranges from 89.3% to 9.16%. Taking into account that the battery consists of 10 cells in series, no cell voltage drops below 3.2V and each of them as well as the overall battery remain in "healthy" operational level.

Additionally to the experimental measurements performed on the developed battery pack, a simulation model was utilized in order to validate battery's performance. The battery model was developed in MATLAB®, Simulink® (Fig. 7) and on the battery equivalent circuit theory. Specifically, a first order equivalent circuit is assumed for the modeling of the battery where battery internal resistance and a parallel RC term in series with the open circuit voltage (OCV) are the degrees of freedom. The OCV is a SoC dependent voltage source. Also, temperature dependence is included in the model in the form of look-up tables providing the values of resistances and capacitance of the model. The battery is placed as the source of the powertrain which is completed with bicycle electric motor. The dynamic behavior of the bicycle is included in the model by means of the following equation that defines the mechanical power, P, required by the motor with respect to the road slope, θ, the bicycle and rider's mass, m, bicycle's aerodynamic drag coefficient, C_b, and frontal area, A, rolling resistance coefficient, f, and bicycle speed, v.

$$P = mv\dot{} + mfg\cos\theta\, v + mg\sin\theta\, v + 0.5C_b\rho Av^3 \qquad (3)$$

All terms in the aforementioned equation can be estimated for each of the experiments performed and inserted in the model. The simulation model has appeared to be quite in accordance with the experimental results as far as the battery SoC concerns. In Fig. 8, an indicative comparison of the SoC and voltage measurement performed for the cases of 15km/h speed by the lighter rider with those resulted from the corresponding simulation are presented. The relative error does

not exceed 2% for both cases except excessive voltage drops which seem to be much more intense for the measurement data. It must be mentioned that errors occurred are the outcome of inaccuracies produced by both the SoC estimation algorithm (Coulomb counting) followed during the measurement procedure and model inaccuracies like the use of first order equivalent circuit and non optimized data for the estimation of battery model degrees of freedom through lookup tables.

The overall battery system is composed of the battery cells stack, a passive battery management system (BMS) to ensure cell balancing during charging and discharging, a temperature measurement circuit, a controller, monitoring battery operation, and a display. As it is developed to provide electric power to human powered vehicles, it was initially selected to be adjusted to the electric bicycle of Fig. 1, supporting 5 levels of electrical assistance for the rider and meeting the requirements of current European legislation [3], that is not exceeding the speed of 25km/h. Assuming a bicycle rider of 85-115kg and taking into account the fact that, on a typical asphalt flat road, 50Wh provide a range of 10km, bicycle autonomy was selected to be around the average value of 50 km [2]. The degrees of freedom in the design are totally focused on the battery system, which determines bicycle autonomy, assuming it is moving only on electric power, and all monitoring parameters. Thus, the battery was designed in order to have nominal capacity around 14Ah and nominal voltage 36V, equal to the nominal voltage of the electric motor selected for the bicycle.

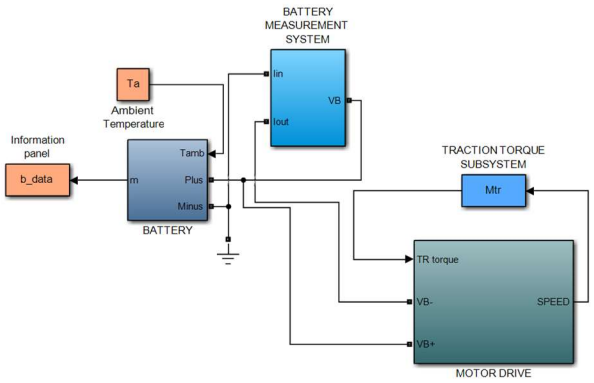

Fig. 7. Simulation model of the e-bike powertrain.

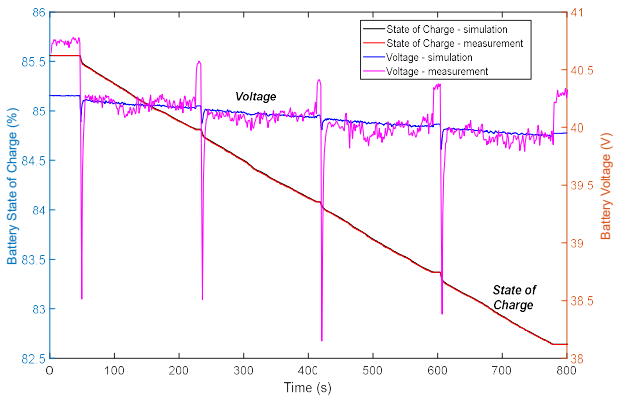

Fig. 8 Comparison of measurements and simulation.

The cell types selected for the battery pack are the Panasonic NCR18650PF Li-ion 18650 cells [4], having as nominal specifications 3.6V voltage, 2900mAh capacity, 1C discharge rate and 3.5C maximum continuous discharge rate. In order for the overall battery to provide 36V voltage and about 14Ah capacity (14.5 to be precise), fifty cells were connected in a 10s5p structure. This kind of structure is able to provide 14.5A nominal discharge current and 50.75A maximum continuous current to the motor, values that are considered adequate for the operation of the electric motor selected. The battery cell pack was cold welded by means of aluminum foils and enclosed in a 3D printed case made of biological Polylactic Acid (PLA) filament, appropriately designed so as to fulfill all technical and space limitations. Together with the battery itself, the temperature measurement circuit as well as the BMS were installed in the PLA enclosure, thus forming the complete battery pack (green structure of Fig. 2).

The measuring and monitoring system records the crucial measures connected to the battery, that is cell voltage for all battery cells, overall battery voltage, battery discharging and charging current, temperature per cell and ambient temperature are measured instantaneously, allowing complete monitoring of battery's state of operation. These values are utilized for the calculation of the instantaneous State of Charge (SoC) which appears on the indication display located on the steering wheel of the bicycle as shown in Fig. 1 and Fig. 3.

IV. Conclusion

An energy storage system appropriate for commercial electrically assisted human powered vehicles is presented in this paper. The battery system is composed of all the essential elements required to provide power assistance to the rider and at the same time measure critical parameters, like battery and cell voltages, electric current, cell temperatures and estimate instant state of charge. A series of measurements are performed by means of a bicycle on which the system is installed. The system is validated by comparison with an appropriately developed simulation model. Although the results are proved to be good, an apparent extension of this work would be the extraction of more load profiles across a wider temperature range, thus creating a database that could be used in order to optimize utilized battery simulation model. Simultaneously, Coulomb counting SoC measurement can be replaced with a more sophisticated algorithm.

References

[1] E. Salmeron-Manzano, F. Manzano-Agugliaro, "The electric bicycle: worldwide research trends," *Energies*, vol. 11, p. 1894, 2018.

[2] A. Muetze, Y.C. Tan, "Electric bicycles: A performance evaluation," *IEEE Industry Applications Magazine*, vol. 4, pp. 12-21, 2007.

[3] EN 15194:2017 (Cycles. Electrically power assisted cycles. EPAC Bicycles). Available from: https://www.en-standard.eu

[4] *Panasonic Lithium Ion NCR18650PF datasheet*, Panasonic Inc., June 2016.

[5] I. Baccouche, S. Jemmali, A. Mlayah, B. Manai, N.E. Ben Amara, "Implementation of an improved Coulomb-counting algorithm based on a piecewise SOC-OCV relationship for SOC estimation of Li-Ion battery," *International Journal of Renewable Energy Research*, vol. 8, pp. 178-187, 2018.

Configurable voltage transformation for energy harvesting with the LTC3109 IC

Dimokratis D. Tsalikis[1] and Michail E. Kiziroglou[1,2]
[1]International Hellenic University
[2]Imperial College London

***Abstract*—This paper introduces the design, analysis and creation of an energy harvesting device with the use of the LTC3109 IC. Nowadays the micro-electronics field has a constant demand for power on small electronic devices with small loads, especially on real time based applications where a full time uninterruptable power source is required. This problem is often tried to be solved with the use of big battery banks which also require physical space, have a decent amount of weight and are sometimes not a viable solution. Also the area in which our power hungry devices are used, can differ, such as sea based applications which introduce humidity and require waterproof solutions, or remote places where the employment of servicing personnel is not possible, such as high altitude mountains or antennas. For these particular reasons, energy harvesting integrated with storage provides an attractive solution. The electrical power provided can be very small depending on the conditions met, but with the use of an external super capacitor or battery, we can constantly charge our power banks, and be ready to feed our power needy device. In applications involving small and bipolar ΔTs, the voltage output of thermoelectric generators (TEGs) requires bipolar handling. For this purpose, integrated DC/DC converters such as the LTC3108 and LTC 3109 are available. In order to cold-startup from voltages below 100 mV, the circuits used involve a pair of switched transformers which however result in adequate efficiency only within a narrow voltage range. To address this problem this work presents a board offering switching among three different pairs of transformers. In this way, the user can select the transformer ratio that is optimum for a given application scenario and environmental ΔT range.**

***Keywords* – LTC3109; energy harvesting; peltier unit; dc/dc converter;**

I. INTRODUCTION

Nowadays electronic devices go even smaller and become more energy efficient than they were some years ago. Although this is true, the problem for indefinite energy supply has not be solved, but there are modern solutions which can help us when we need to use small electronic loads for long periods of time. For environments experiencing varying and bipolar temperature differences (ΔT) such a solution can be found in the combination of a thermoelectric generator (TEG) with a bipolar, low voltage DC/DC converter circuit such as the LTC3109 [5]. This work presents such an implementation, with a board with the unique feature of including three voltage step-up transformers, available for the board user to select in order to maximize efficiency for a given environment and corresponding ΔT.

II. CIRCUIT DESIGN

Initial thoughts

The first idea was to design a circuit that would be sufficient to use on both low and high input voltages, thus harvesting as much power as possible. The circuit schematic implementing the three selectable transformer pairs approach is presented in Figure 1.

SMD Transformer pairs

The user can select between 3 different transformer pairs, each with their own ratio of 1:10, 1:50, 1:100. A 1:10 ratio would be used if our input power was big enough and a 1:100 in the case of low voltage, from 100mV and below. By doing this we reduce losses due to transformer windings, inductances and capacitances with the near environment, thus improving efficiency.

Internal circuitry

After the internal circuitry of our IC is supplied with power, dc/dc conversion takes place, in combination with an internal reference voltage and a linear regulator, thus providing the power at a higher voltage level on our outputs.

III. CIRCUIT SIMULATION

A simulation of the circuit was performed, in order to analyze it and see the possible scenarios that we would get optimal results. The three most important things that we should know, is the input resistance, the output resistance and the efficiency of our circuit. Results of simulated efficiency for different input voltages and load resistors are presented in Fig. 2. Furthermore, load-matching at the output was studied, and a total circuit output resistance of 65 Ω was measured (Fig. 3).

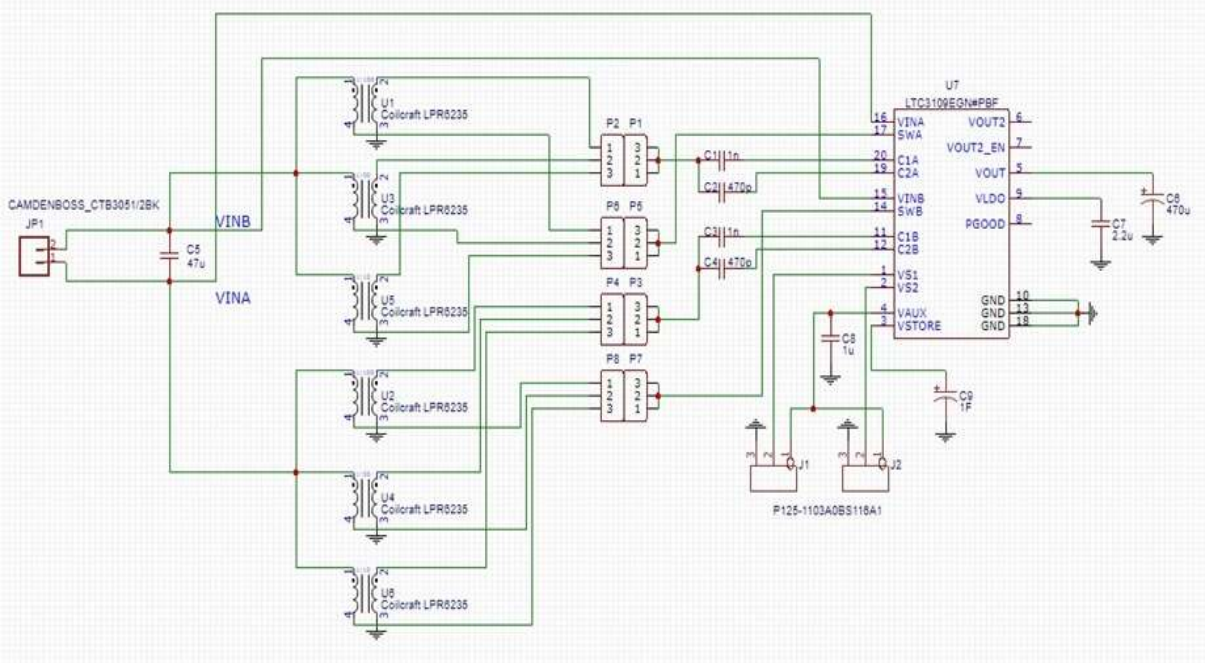

Figure 1. Circuit schematic

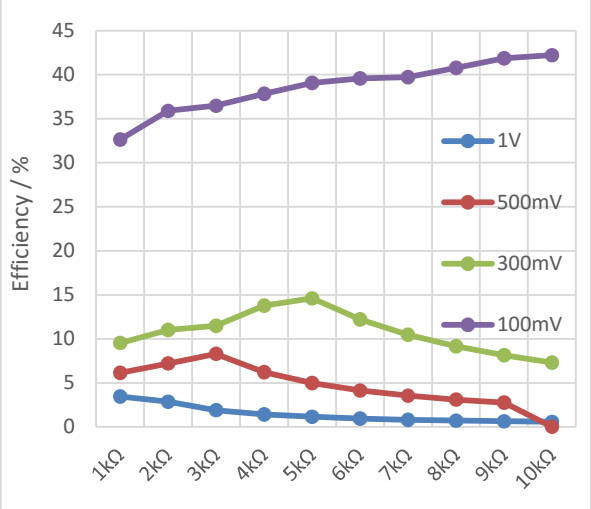

Figure 2. Efficiency / Vin / Output Resistance(kΩ)

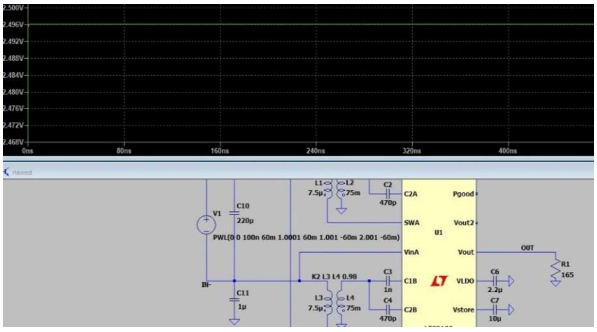

Figure 3. Output resistance measurement setup

IV. Experimental Details

PCB Design

The design of our PCB was made using a cloud based service called EasyEDA [1]. The PCB board was printed by a company called JLCPCB [3]. The circuit layout is presented in Fig. 4. The components of the PCB were hand soldered using a soldering station and a hot air station. Photographs of the main components used are shown in Fig. 5.

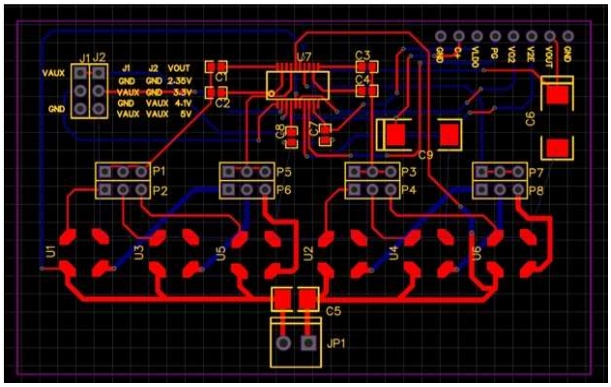

Figure 4. PCB Blueprint

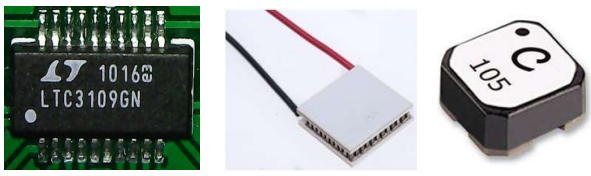

Figure 5. Left: Soldered LTC3109 IC, Middle: Peltier unit (TEG), Right: SMD Transformer.

Component soldering

Using a soldering station in combination with solder paste and hot air for the SMD parts, the process was easy with great results. The final PCB assembly is shown in Figure 6.

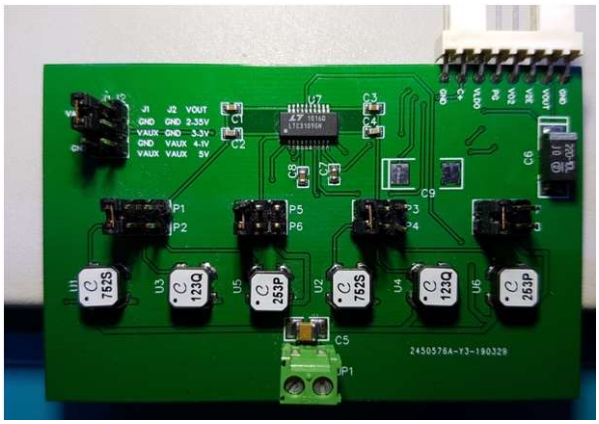

Figure 6. The assembled board

V. EXPERIMENTAL RESULTS

After the completion of our board, a TEG [4] was used for the input voltage, a slight heating on one side with the help of a heat gun, in combination with a PCM filled with water for the cooling of our cold side, as introduced by the authors of the paper [6]. The results were satisfying, since our outputs could hold a decent charge, and even charge an external super capacitor of 1F (Fig. 6). Considering the use of such an application in a real-life situation, the whole process of charging and regulating would be much slower. Nevertheless, this charging may be a critical contribution considering that an electronic device such as an airplane black box could be able to keep on reporting its signal for a long time.

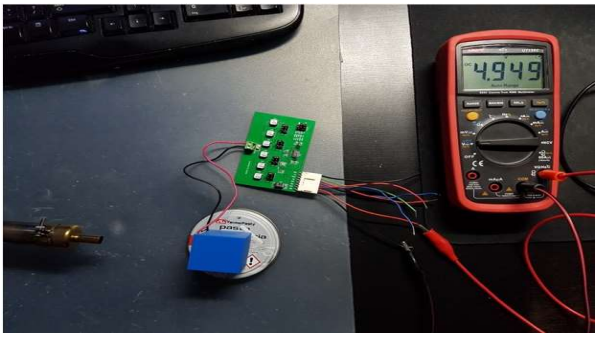

Figure 6. Super-capacitor of 1 F charged to 4.9 V by a TEG through the proposed circuit.

REFERENCES

[1] EasyEDA PCB Design, https://easyeda.com/
[2] LTSpice, https://www.analog.com/en/design-center/design-tools-and-calculators/ltspice-simulator.html
[3] JLCPCB, https://jlcpcb.com/
[4] TEG, https://www.electron.com/peltier-module-hebei-tec1-12705-p236/
[5] LTC3109, https://www.analog.com/en/products/ltc3109.html
[6] M. E. Kiziroglou, Th. Becker, S. W. Wright, E. M. Yeatman, J. W. Evans and P. K. Wright, 3D Printed Insulation for Dynamic Thermoelectric Harvesters with Encapsulated Phase Change Materials, IEEE Sensor Letters, 1 (4), 1-4, 2017

Embedded Systems from Industry's view

Dimitris Vamvatiras, Theodoros Geladaris
R&D Department, Semitron S.A., Thessaloniki, Greece

***Abstract* — The purpose of this paper is to provide an overview of Embedded Systems meaning, and their role in the products of Semitron S.A. company. In the first part of this paper, the company profile of Semitron S.A. is briefly presented. In the second and third part, the general concept of Embedded Systems is described and analyzed, along with some references related to Semitron's way of development as well as to a complex product designed and developed by Semitron's R&D Department.**

I. SEMITRON S.A. PROFILE

Semitron S.A. was established in 1978 in Thessaloniki and operates in company-owned, fully equipped facilities in the industrial area of Sindos, Thessaloniki. In the next years, business was expanded in Athens, Ireland, Turkey and Algeria with subsidiary companies. Semitron is a rapidly developing company currently present in 25 countries around the world, while its reputation is growing.

The company policy is based on 4 levels:

- Quality & Reliability (certified by ISO9001)
- Services (superior quality and unparalleled reliability)
- Design (specialized solutions that meet every need or aesthetic demand)
- Flexibility (adjustment of the corporate mechanism to the international needs)

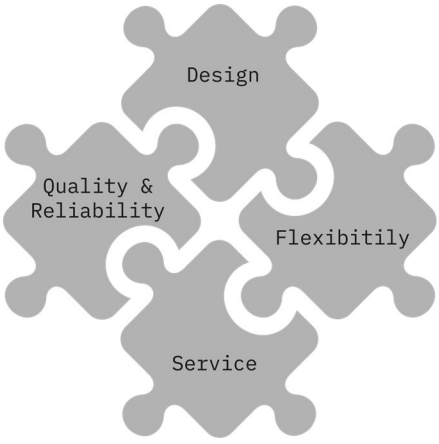

Fig. 1. Company Policy

Every product is entirely created by Semitron in terms of software and hardware, something that gives the company the ability to be flexible and to adjust to individual customer needs. The company's fully automated production line and the privately owned testing laboratories ensure a consistently high quality level of manufactured products, which are certified by qualified European institutions.

Some of the main products are:

- Taximeters
- Android Industrial PC
- Thermal Printers
- Lift Control Units
- Fiscal Solutions
- Data managing systems (Bluetooth, NFC, i-Button, RFID, etc)
- Applications (Desktop, mobile, web)
- Databases

Fig. 2. Some of Semitron's Products
(Pictures are in demonstration scale)

Semitron's goal is to deliver reliable products of unique design which will exceed customers' expectations. The vision is to improve people's lives through technology and innovation.

II. Description of Embedded Systems

Embedded systems are a major part of Semitron's R&D work. An embedded system is a combination of hardware and software, designed for a specific function or functions within a larger system. Taximeters, lift control boards, medical equipment, household appliances and vending machines as well as mobile devices, host an embedded system.

Embedded systems are computing systems that range from having no user interface (UI) to complex graphical user interfaces (GUIs) such as in mobile phones. Semitron develops various devices which indeed differ in complexity.

The decision to initiate a UI design may apply on simple requirements -like developing a simple telematics device for data transmission with an easy user interface of 3 indication LEDs or to implement a 5" TFT Display interface, using touch panel for navigating the device combined with an advanced graphics user interface.

A. *Embedded Software*

Software developed for embedded devices is called Embedded Software. The use of embedded software is a rapidly growing field. The importance of the applications developed varies depending on the application and its features. As the electronics industry continues to produce new electronic materials that are faster and can handle even more functions, the use of embedded software will continue to grow.

In Embedded Systems, quality plays a key role in cost efficiency and cost improvement. Finding and resolving code bugs is overall the most expensive software development activity. Quality leads, and productivity follows.

In Semitron the bigger part of Embedded software is written in Embedded C and C++ using various commercial compilers (Keil, IAR, CodeWarrior etc).

B. *Embedded Hardware*

In general an embedded system may consist of a microcontroller with a few extra auxiliary components or may consist of multiple microcontrollers and electronic circuits operating in parallel. However, even when the components of an embedded system are different, the principles underlying its design are the same.

The hardware of an embedded system is nothing more than electronic components and circuits designed to move, store and change numbers. At the heart of the computer system is the processor responsible for executing programs, while another key component is the memory used to store programs and data. Finally, the software controls system operation and functionality by essentially controlling the hardware.

In the products of Semitron a wide variety of microcontrollers are used. The final choice is not always an easy task. Even nowadays where powerful microcontrollers with various peripherals are available, someone should be careful in the final decision. Many different parameters should be taken into account (price, maturity, availability, investment, hardware architecture, processing power, etc).

C. *Embedded Systems Architecture*

Each embedded system is characterized by a specific architecture that relates to a simplified representation of the system and does not include detailed components such as software source code or electronic circuit design. At the level of system architecture, hardware and software are presented as components that simply interact with each other.

Figure 3 shows a diagram of an embedded system model. This model indicates exactly the fact that all embedded systems share a similarity at their lower level. That is the Hardware.

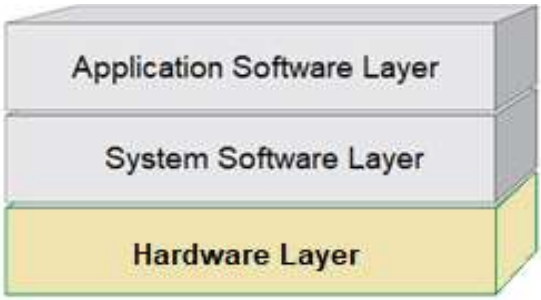

Fig. 3. Embedded System Model

In Semitron, the analysis of the architecture of a new embedded system, takes deep and careful study. The goal is to identify and address challenges, which will be present in the design and development processes, from an early stage. The overall condition consists of a number of elements and parameters, which will determine the final design.

III. NOUS Lift Control Unit

The NOUS lift controller is a high-performance microcomputer, functioning as the main processing unit of a lift control panel. The NOUS application has so many parameterized options, functions and graphics that it requires to run on an Operating System. NOUS is an advanced embedded system, based on the YOCTO project, running a custom-made embedded Linux distribution as its operating system. When running an Operating System like Linux, microprocessors are used instead of microcontrollers because the resources of RAM and speed are very high while microcontrollers can only run small compact size operating systems (e.g. RTOS).

Fig. 4. NOUS Lift Control Board

There are several benefits to using an operating system like Linux, for this type of application. Thanks to its open source nature, it is highly customizable and can provide access to various high level capabilities, as well as being secure, reliable and flexible. A custom made Application written in C++ is responsible for the functionality of the Lift control board.

NOUS is being controlled by a modern touch screen interface providing comprehensive overview and navigation over the whole elevator (lift status, doors status etc.), as well as, easy access to service and maintenance functionality (event log, inspection mode etc.). The whole board consists of five different PCB boards:

- CPU and I/O boards on the top side
- Safety Chain and Safety Circuit boards on the bottom
- Expansion board which is connected to the CPU board and can be placed anywhere in the control panel

A simplified block diagram of NOUS CPU board is given below.

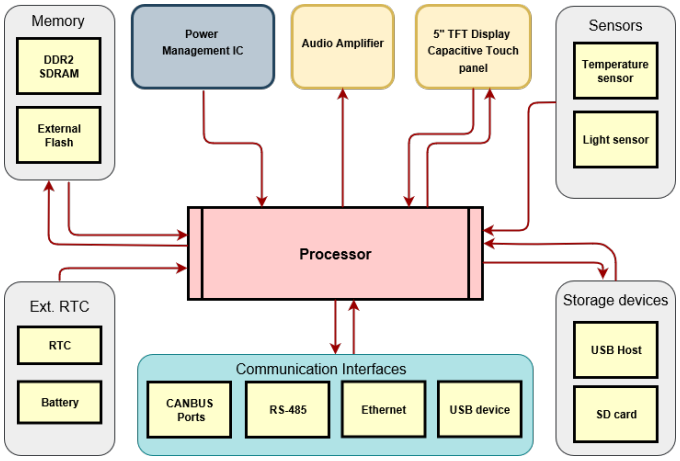

Fig. 5. Simplified Block Diagram of NOUS CPU board

The main components of NOUS CPU Board are:

Processor	ARM Cortex-A5 SAMA5D36 324 Pin BGA Package
RAM	2 x 1Gb DDR2, 800MHz Clock Speed
External Flash	2Gb NAND Flash
CANBUS	2 x Isolated CAN bus ports
Display	5" TFT Display Resolution of 800x400 Pixels 24bit RGB interface Capacitive touch panel

IV. Copyright

References

[1] Steve Heath, (2003). *Embedded Systems Design, Second Edition*. Newnes.

[2] Tammy Noergaard (2013). *Embedded Systems Architecture, Second Edition.* Newnes.

[3] Theodoros Geladaris, (2016). *Agile Management of an Embedded Systems R&D department*, Hellenic Open University.

[4] Bart Broekman and Edwin Notenboom, (2003). *Testing Embedded Software.* Addison Wesley, 2003. 94

[5] Ebert C, Jones C, (2009). *Embedded software: Facts, Figures, and Future.* IEEE Computer Society. 2009 ;42(4):42-52.

[6] John Koon, (2019). Key factors to consider when choosing a microcontroller https://www.microcontrollertips.com/key-factors-consider-choosing-microcontroller/

[7] Margaret Rouse, (2018). *Embedded System.* https://internetofthingsagenda.techtarget.com/definition/embedded-system

[8] Thor Engineering https://www.thor.engineering/

Prototype Power Supply Solutions for a Gel Electrophoresis Apparatus

D. Triantafyllidis[1+], N. Nikolaidis[1], N. Evgenidis[1], D. Bechtsis[1], Ap. Tsagaris[1], A. Filelis[2], S. Papaoikonomou[2], F. Stergiopoulos[1]

[1] International Hellenic University / Department of Industrial Engineering & Management
P.O. Box 141, 57 400 Sindos, Thessaloniki, Greece
[2] Evresis S.A, DA 12a Block: 39b Industrial Area, 57400, Sindos, Thessaloniki, Greece

[+] Corresponding author: drdimitri@autom.teithe.gr

***Abstract* — The present paper presents the design of two solutions for a power supply suitable for supplying the necessary power, under suitable voltage and current conditions, to a gel electrophoresis apparatus. Special design considerations had to be addressed in order to accommodate the specific requirements of the electrophoresis procedure. Two approaches are presented, of which one is a case-specific custom design and the other uses readily available parts from the market. The implementation of the gel electrophoresis apparatus is still in progress, therefore no lab results could be attained at this point. Nevertheless, it was favorable to implement the second approach, with very promising results.**

I. Introduction

Biomolecules are frequently electrically charged, which, therefore, when placed in an electric field, move towards the electrode of opposite polarity due to the phenomenon of electrostatic attraction. Electrophoresis is the separation of charged molecules in an applied electric field. The relative mobility of individual molecules depends on several factors, of which the most important are charge, mass, molecular shape and the temperature, viscosity and porosity of the medium through which the molecules migrate [1]. Complex mixtures of molecules can be resolved to very high resolution by this process [2]. There are several modes of applying the electric field to the medium, according to desired results, as presented in Table I.

Table I: Modes Of Operation.

Mode	Description	Results
Constant Power	Power (VI) will be held constant, but voltage and current will vary.	Mobility of samples will be unpredictable but the generation of heat will remain constant.
Constant Current	Current (I) will be held constant, but voltage and power will vary.	Samples will migrate at a constant rate, but voltage and power will increase as the resistance increases, resulting in an increase in heat generation.
Constant Voltage	Voltage (V) will be held constant, but current and power will vary.	The current and power will decrease as the resistance increases, resulting in a decrease of heat and samples migration.

In the present paper the medium is a horizontal agarose gel and the biomolecules are human blood samples migrating in one dimension. This type of electrophoresis is known as 1D AGE (One Dimension Agarose Gel Electrophoresis). The required mode of operation is constant voltage. In this mode the applied electric field is kept constant, but because the resistance of the agarose gel is expected to increase with running time the current is expected to decrease, resulting also in a reduction of heat dissipation with time. The mobility of the biomolecules will also be affected detrimentally, with decreasing current, but this mode of operation is accepted as an industry standard in these types of electrophoresis apparatus, leading to widely acceptable and commonly interpretable results.

II. Design Criteria

The power supply should meet at least the following design criteria for the requirements of the AGE apparatus:

- Output voltage range: 75…200 V DC
- Output current: up to 250 mA
- Output power: up to 50 W
- Controllable through a computer interface

The AGE apparatus will be required to run the following programs, according to Table II:

Table II: Required Programmes.

#	Duration (min)	Voltage (Volt)	Test type
1	20	100	Proteins
2	20	200	Hemoglobin's in alkali
3	22	100	Lipoproteins
4	25	75	Hemoglobin's in acid
5	20	100	Immunofixation IFE01
6	18	100	Immunofixation IFED01
7	50	150	A-Amylase Isoenzymes
8	25	150	Alkaline Phosphatase
9	manual	manual	User defined

Voltage stability was at first addressed quite strictly, but research and feedback from the electrophoresis users community revealed that even very loosely standards do

not lead to a perceivable deterioration of the quality of the results. This is not surprising, since a variation in the applied electric field will exert a proportional force variation to all migrating biomolecules, changing only their absolute, but not their relative final position on the agarose gel. Hence, a criterion of ±5% variation was set, which can be easily obtained with no special design considerations.

III. The Proposed Power Supplies

Power supply A is based on a custom-made approach, where the whole design has been carried out using a design and simulation software from Texas Instruments [3]. Various discrete electronic and IC components are combined until a simulation of the circuit under consideration validates the required design parameters.

Power supply B is based on a system integration approach. In this case already available parts, not specifically designed or produced for the scope of gel electrophoresis, where selected and integrated into a final solution that met the design criteria. Power supply B was actually implemented and operated, which was not a goal pursued for Power supply A at this point of the ongoing research.

A presentation of each design follows.

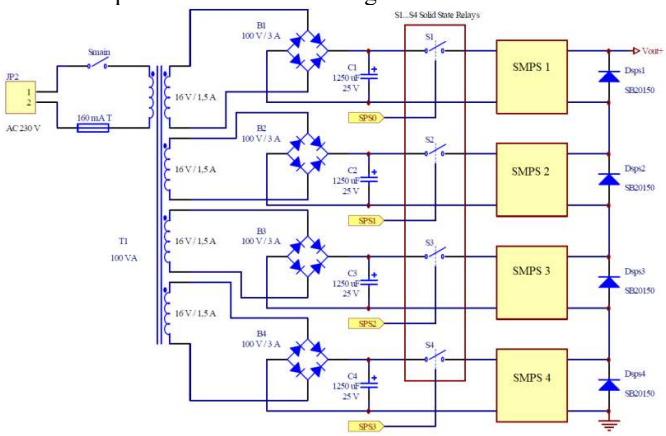

Figure 1. Block diagram of power supply A.

IV. Power Supply A

A block diagram of the design of power supply A can be seen in Figure 1. It is a multi-stage design based on four modules of the same switched-mode power supply (SMPS) [4] connected in series. The reason for not proceeding with one SMPS for the complete range of voltages is that it was found that stability problems could arise. The available ICs on the market are offered on the basis that large voltage input variations should lead to a constant output voltage within a small user-selectable range. However, in the presented design the requirements are for an output voltage with a very large user-selectable range, from 75 up to 200 Volts. Another constrained that lead to the consideration of this design was the unavailability of freely selectable coil inductances. In most design scenarios examined, with a large output voltage selectable range, the required inductances calculated where not available in the market and would be required to be custom-made, thus increasing the cost. This was ruled out as an option from the very beginning.

Therefore, it was decided to proceed with four modules of the same SMPS, each of which has very favorable stability behavior and excellent technical specifications within an output voltage range of 30…64 Volts and can be easily manufactured from parts readily available in the market. By connecting the four supplies in series a voltage range of 30…256 Volts can be attained which is even more than required. Each of the four SMPS is based on the LM5022 Integrated Circuit from Texas Instruments. The schematic is presented in Fig. 2.

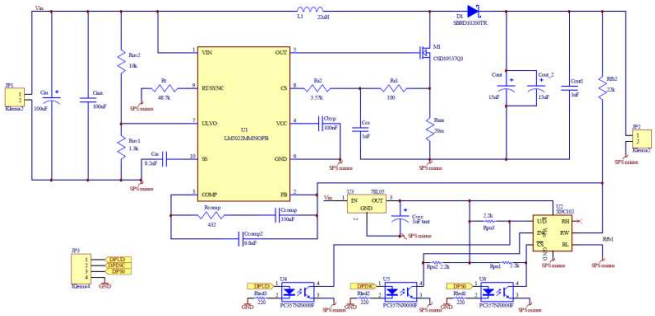

Figure 2. Schematic of one of the four SMPSs. In the down right corner the digital potentiometer U2 of type X9C102P (by Intersil) to select the output voltage can be seen.

Fig. 3 presents four interesting obtained design results, as calculated by the Texas Instruments simulation software [3], namely:

(a) Efficiency according to load conditions. As can be seen excellent efficiency above 88% is possible even under worse low load conditions.

(b) Output voltage vs. time. For V_{DC}=63.48V an extremely small variation of the output voltage can be observed with a peak to peak value of 185.6mV. This corresponds to 0.29%, which is minimal.

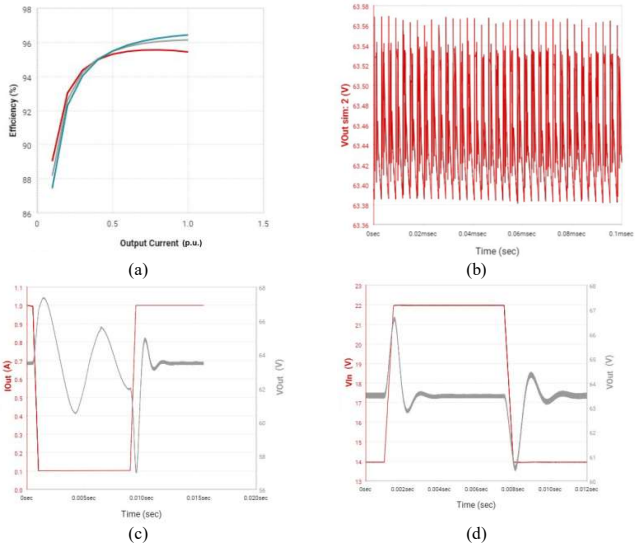

Figure 3. Simulation results. (a): The efficiency of the SMPS, (b): Time evolution of output voltage, V_{DC}=63.48V, V_{ACp-p}=185.60mV, (c): Load disturbance, (d): Input disturbance.

(c) Step-function load disturbance. Overshot settling time is 7.96ms and undershot settling time is 1.88ms. Overshot and undershot voltages are 67.38V and 56.96V, respectively, with V_{DC}=64V, leading to a 5.28% and -11% disturbance of the output voltage.

(d) Step-function input voltage disturbance. Overshot settling time is 1.7ms and undershot settling time is 2.58ms. Overshot and undershot voltages are 66.71V and 60.41V, respectively, with V_{DC}=63.5V, leading to a 5.06% and -4.87% disturbance of the output voltage.

All obtained simulation results were excellent and well within the requirements of the design parameters.

The block diagram of Fig. 1 is in open loop. In the final design a closed loop will be implemented. For this purpose a micro-computer will be fed with voltage and current from the output stage in order to drive each of the SMPSs in parallel, by controlling all four of the digital potentiometers at once (see Fig. 2).

A manufacturing cost analysis for this design showed that for one unit only the cost would well exceed 800 Euros, but for 100 units the cost would significantly drop to about 150 Euros per unit, casings excluded. Of course, the cost per unit would drop even further should higher quantities be required.

V. Power Supply B

A schematic of Power Supply B can be seen in Figure 4. The main component is a lamp dimmer [5], which can produce variable output AC voltage for various types of lamps and LEDs. The produced AC voltage is then rectified and stabilized, producing a freely selectable DC output voltage.

The selected dimmer used is EUD12DK from the company ELTAKO, which although oversized was available at a very competitive price. This 800W dimmer is capable of driving even inductive loads, such as transformers. G1 is a four diode industrial grade rectifier. G2 is a simple power supply for the power requirements of a micro-computer and C1 is a voltage stabilizing capacitor which was chosen to have a capacity of 4700μF in order to minimize ripple. The components are enclosed in an industrial grade enclosure. The micro-computer is responsible for producing the required PWM signal to drive the dimmer. A feedback network was not introduced at this point, because the scope of this implementation was to have a "proof of concept." Since the microcomputer is already a required part of the design it is straight-forward to use a shunt resistor in series with the output to sense the output current, as well as the output voltage in conjunction with a buffering circuit, in order to generate a floating feedback signal for the microcomputer. This part is left out at this point as future work.

The proposed configuration was assembled using easily obtainable parts and has been empirically tested to produce acceptable results. A thorough investigation of the behavior of the circuit was not in the scope of the present work and is left as future work. The cost of the manufactured unit was about 250 Euros, without casing, of which more than half are due to the dimmer and the output capacitor. A mass production would lead to a drop in cost, but since more than half of the cost is in materials with mostly rigid prices, the production cost cannot be reduced significantly.

VI. Conclusions and Future Work

Two solutions are proposed for the design of a One Dimension Agarose Gel Electrophoresis apparatus power supply. The first solution (power supply A) is a bottom up design, completely custom engineered for the needs of the proposed application. This designed is very promising in regards of specifications, exceeding in simulations the design criteria by much. This solution is complex to implement in a one-off basis and is rather favorable for a large scale production, since it can be customized and optimized accordingly, leading to a cost effective mass production. In addition this solution has the advantage of small physical size.

The second solution (power supply B) is made by integrating readily available parts from the industrial electronics and electrical installations market. The implementation is rather straightforward, easy and fast and introduces no difficulty or surprises. In comparison to power supply A it is rather expensive and is preferred as a one-off solution in cases where a power supply is required immediately in small numbers.

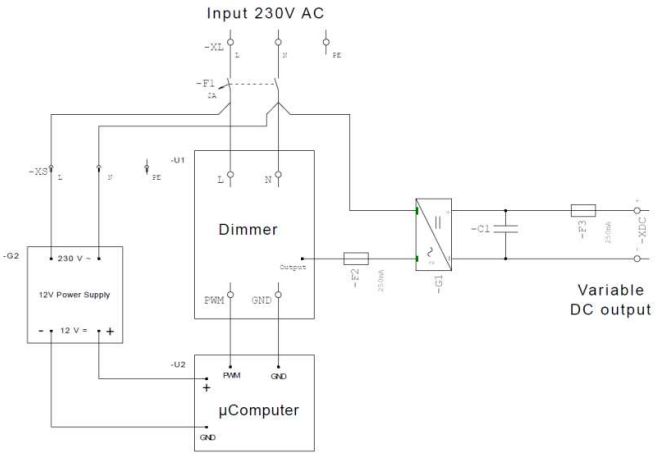

Figure 4. Schematic of Power supply B.

Future work will allow the physical implementation of power supply A as well, and its lab comparison with power supply B in order to facilitate a one to one real-world comparison between the two solutions, where the feedback circuits will also be included in both designs.

VII. Acknowledgments

This research has been co-financed by the European Regional Development Fund of the European Union and Greek national funds through the Operational Program Competitiveness, Entrepreneurship and Innovation, under the call RESEARCH – CREATE – INNOVATE (project code: T1EDK-02403).

References

[1] Sameh Magdeldin, Editor, "Gel Electrophoresis – Principles and Basics," InTech, 2012.

[2] Sheehan, D., "Physical biochemistry: Principles and applications," John Wiley and sons, 2000.

[3] WEBENCH ® Power Designer, http://www.ti.com/design-resources/design-tools-simulation/webench-power-designer.html

[4] Wei-Hsin Liao, Shun-Chung Wang, Yi-Hua Liu, "Learning switched mode power supply design using MATLAB/SIMULINK," TENCON 2009 - 2009 IEEE Region 10 Conference.

[5] Andrew Penfold, "Dimmers," Wiring Installations and Supplies (Volume: 1984, Issue: 21, November-December 1984), IET.

Acoustic Power Transfer Through Structures

Michail E. Kiziroglou[1,2], Akshayaa Pandiyan[2], David E. Boyle[2], Steven W. Wright[2] and Eric M. Yeatman[2]
[1]International Hellenic University, Greece
[2]Imperial College London, U.K.

Structural health monitoring often requires a large number of sensors. Their powering is challenging because of the high maintenance cost associated with the recharging requirement of batteries, the unreliability of power status and often the inaccessibility at remote sensing locations. To address this challenge, energy harvesting and wireless power transfer technologies have emerged in recent year, demonstrating adequate energy and power densities for portable powering, but their industrial applicability is currently limited by the requirement for customization in each specific environment and application. In this work we present an experimental demonstration of the viability of acoustic power transfer through metallic pipelines, for powering remote sensor nodes (Fig. 1, Left). The results show power transfer of 18 mW at a pipeline distance up to 1 m. The effect of liquid filling is investigated and the timing of wave packet arrival to the power receiver is analysed (Fig. 1, Middle). The discussion is complemented with an outlook about power increasing techniques including wavelength-matching acoustic interfacing as well as acoustic and electrical impedance matching, and a brief summary of power distribution systems that could be benefitted by acoustic power transfer technologies (Fig. 1, Right).

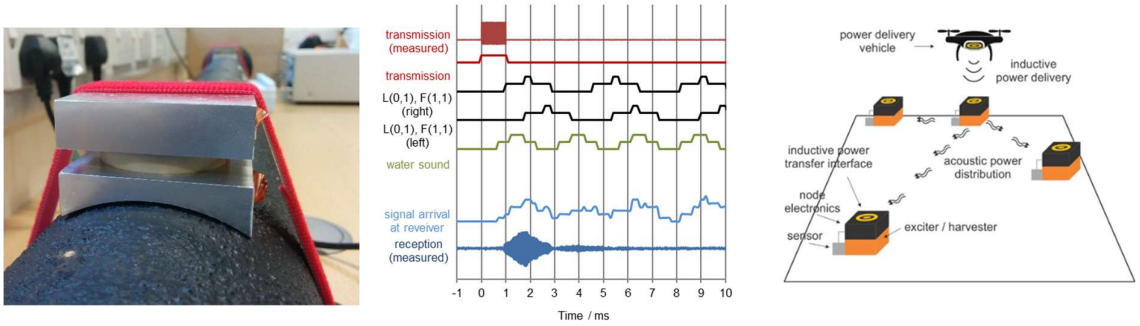

Figure 1. Left: A bulk PZT transmitter for acoustic power transfer through pipelines [1]. Middle: Simulated timing of acoustic packet arrival to receiver in comparison with measurements from pulsed wave tests [1]. Right: A combined drone-to-sensor inductive power transfer and local acoustic power transfer scheme [2].

References

[1] M. E. Kiziroglou, D. E. Boyle, S. W. Wright and E. M. Yeatman, Acoustic power delivery to pipeline monitoring wireless sensors, Ultrasonics 77, 54–60, 2017.
[2] A. Pandiyan, M. E. Kiziroglou, D. E. Boyle, S. W. Wright and E. M. Yeatman, Optimal Energy Distribution Using Clustering Algorithm, PowerMEMS, Krakow, Poland, Dec. 3-6, 2019.